MATERIALS SCIENCE

Molecular defect-containing bilayer graphene exhibiting brightened luminescence

Xin-Jing Zhao*, Hao Hou*, Peng-Peng Ding, Ze-Ying Deng, Yang-Yang Ju, Shun-He Liu, Yu-Min Liu, Chun Tang, Liu-Bin Feng, Yuan-Zhi Tan†

The electronic structure of bilayer graphene can be altered by creating defects in its carbon skeleton. However, the natural defects are generally heterogeneous. On the other hand, rational bottom-up synthesis offers the possibility of building well-defined molecular cutout of defect-containing bilayer graphene, which allows defect-induced modulation with atomic precision. Here, we report the construction of a molecular defect-containing bilayer graphene (MDBG) with an inner cavity by organic synthesis. Single-crystal x-ray diffraction, mass spectrometry, and nuclear magnetic resonance spectroscopy unambiguously characterize the structure of MDBG. Compared with its same-sized, defect-free counterpart, the MDBG exhibits a notable blue shift of optical absorption and emission, as well as a 9.6-fold brightening of its photoluminescence, which demonstrates that a single defect can markedly alter the optical properties of bilayer graphene.

INTRODUCTION

As the seminal two-dimensional (2D) van der Waals assembly, bilayer graphene exhibits a variety of unique electronic and optical features not available in single-layer graphene, such as bandgap opening (*1*), bound exciton (*2*, *3*), superconductivity (*4*–*7*), etc. Similar to other graphenic materials (*8*–*10*), the hexagonal carbon lattice of bilayer graphene could be dotted with heterogeneous natural defects, which can play a key role in modifying the physical and electronic properties of the material (*11*–*14*). The generation of well-defined defects in nanocarbons, particularly in bilayer graphene system, has been a long-standing challenge (*13*, *15*). This is because in the latter case, not only the artificially generated defects need to be homogeneous across the carbon lattice but also the two graphene layers themselves are required to stack in an orderly fashion. As an example, Mugarza *et al.* (*16*) recently described the synthesis of well-defined nanoporous single-layer graphene on the surface by controlled surface-assisted polymerization and cyclodehydrogenation. However, arranging this defect-containing graphene layer into van der Waals stacks remains demanding and challenging (*17*).

Alternatively, well-defined molecular nanocarbon fragments have been widely investigated to deduce the structure-property correlation of carbon nanomaterials. A series of these constructs bearing different types of defects (*18*–*21*), such as vacancies or nonhexagonal rings, have been designed and prepared by organic synthesis, enabling researchers to better characterize and understand the roles that these defects play in modulating the structure and properties of the nanomaterials at the atomic level (*22*). However, to the best of our knowledge, no molecular cutout of defect-containing bilayer graphene (Fig. 1) has been reported. The successful synthesis of molecular defect-containing bilayer graphene (MDBG) demands both synthesizing the molecular fragment with defined defects and assembling two fragments into a discrete bilayer complex. Bilayer molecular architecture can be achieved by tethering two monomers together through a covalent linker, as the first synthesis of covalently linked bilayer nanographenes by Müllen *et al.* (*23*) and Martín *et al.* (*24*). Recently, we developed a strategy to create stable discrete bilayer assemblies of nanographenes by noncovalent interactions (*25*). We reasoned that a similar strategy can be adopted to arrange two defect-containing nanographene molecules into a stable discrete bilayer, which represents a molecular fragment of defect-containing bilayer graphene (Fig. 1).

Here, we report the synthesis of MDBG (compound **1**), which carries a cavity defect at its center. We demonstrate that **1** maintains a bilayer architecture in the gas phase, solution, and solid state. Single-crystal x-ray diffraction (SCXRD) confirms that the structure of **1** consists of a unique bilayer structure with a six-membered ring cavity at the center of its carbon framework. Compared with its defect-free counterpart, **1** exhibits a notable blue shift of photo absorption and emission, corresponding to an enlarged optical HOMO-LUMO (highest occupied molecular orbital–lowest unoccupied molecular orbital) gap by 0.57 eV. Without introducing any heteroatom or chromophore, the photoluminescence (PL) intensity of **1** showed a 9.6-fold enhancement, which serves as the atomically precise case of defect-enhanced PL in nanocarbons. Further, PL dynamics

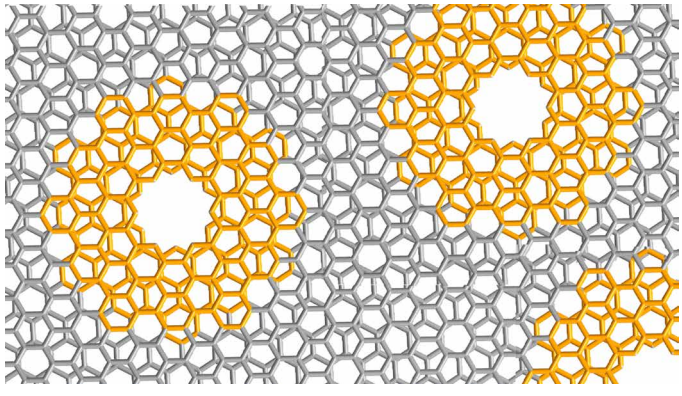

Fig. 1. Molecular cutout of defect-containing bilayer graphene. The MDBG we synthesized (highlighted in orange) can represent the cutout of defect-containing bilayer graphene.

Collaborative Innovation Center of Chemistry for Energy Materials, State Key Laboratory for Physical Chemistry of Solid Surfaces, and Department of Chemistry, College of Chemistry and Chemical Engineering, Xiamen University, Xiamen 361005, China.
*These authors contributed equally to this work.
†Corresponding author. Email: yuanzhi_tan@xmu.edu.cn

discloses a much faster radiative decay rate and a slower nonradiative decay rate of **1**, which can account for the PL enhancement.

RESULTS

Synthesis of MDBG

The synthesis of MDBG entailed the initial construction of a well-defined defect-containing monolayer. To this end, we designed a hexagonal nanographene with an inner cavity as the MDBG monomer and envisioned that its controlled assembly into a stable discrete bilayer could be achieved by decorating mesityl groups at the vertexes. Following this blueprint, we first synthesized hexaborylated [6]cyclo-m-phenylene (*26*) as a template and subjected it to annulative π extension (*27*, *28*). The hexaborylated [6]cyclo-m-phenylene was coupled with 2-bromo-5-mesitylbiphenyl via the Suzuki-Miyaura coupling (Fig. 2A and figs. S1 and S2). The resulting mesityl-functionalized polyphenylene precursor was then cyclodehydrogenated using iron(III) chloride. Because of the peripheral mesityl groups, the monolayer defect-containing nanographene stacks into a discrete bilayer spontaneously, as validated by the characterizations described hereafter.

The matrix-assisted laser desorption/ionization–time-of-flight (MALDI-TOF) mass spectrum of purified **1** showed a single peak with

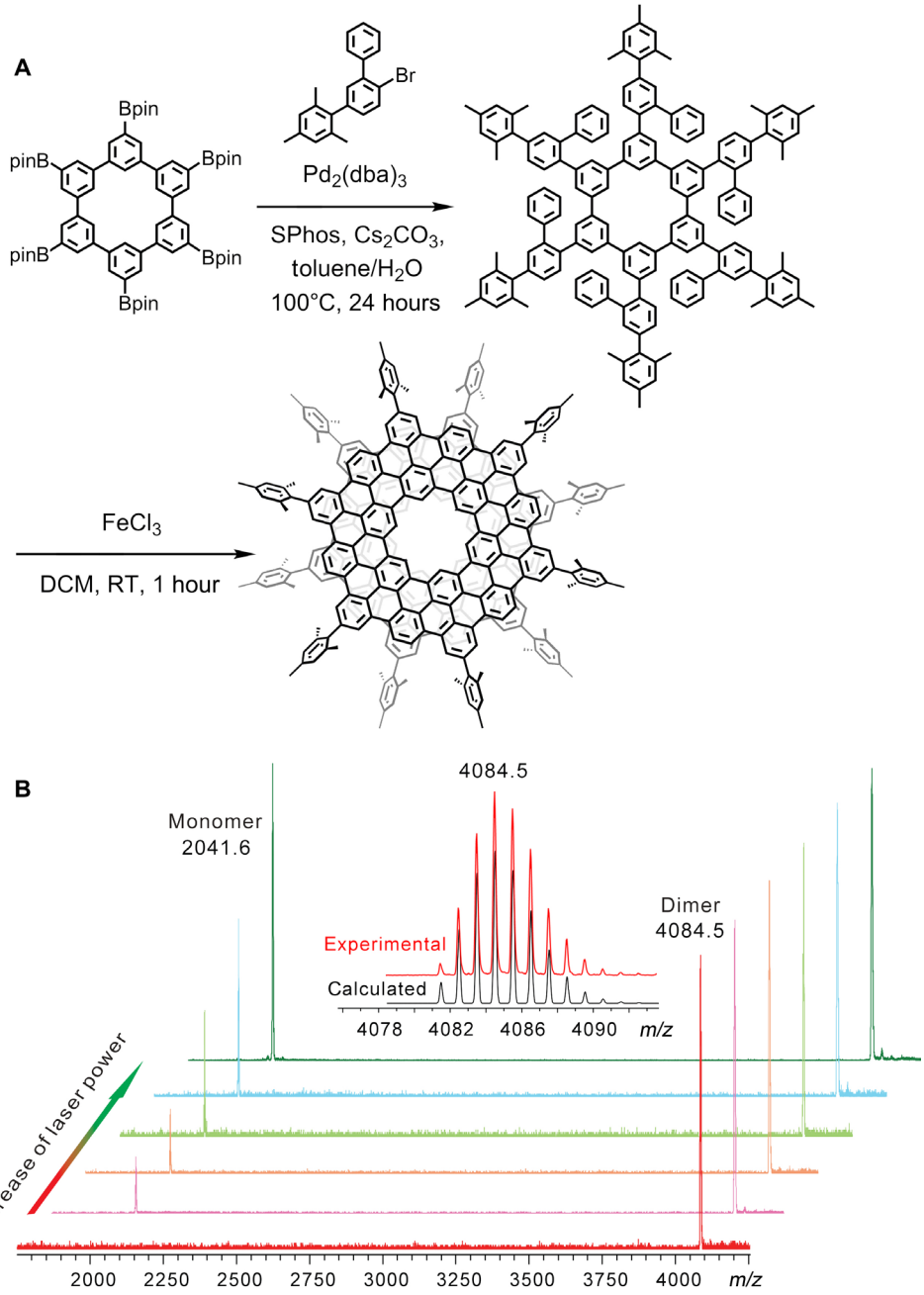

Fig. 2. Synthetic route and mass spectra of 1. (**A**) The synthetic route toward **1**. DCM, dichloromethane, RT, room temperature. (**B**) The mass spectra of **1** with different desorption laser power. The isotopic distribution for the mass peak of **1** is shown as an inset. *m/z*, mass/charge ratio.

its experimental mass/charge ratio value [4084.5 Da, $(C_{108}H_{30}(C_9H_{11})_6)_2$] and isotopic distribution precisely matching that predicted for MDBG (Fig. 2B), supporting the formation of a bilayer structure. The dominance of bilayer signal, as manifested in the spectra, lent credence to the stability of the bilayer in the gas phase (Fig. 2B). A key feature of van der Waals dimers is that they can undergo dissociation when subjected to strong disturbance. Gradually enhancing the laser energy during the MALDI processes resulted in an additional peak at 2041.6 Da, which corresponded to the monolayer fragment $[C_{108}H_{30}(C_9H_{11})_6]$ of **1**, with increasing intensity (Fig. 2B). This further confirmed that **1** was composed of two noncovalently stacked layers.

Crystal structure of 1

The previously reported defect-containing nanographene C_{216} that bears an inner cavity is completely insoluble in the commonly used solvents (*21*), which hampered the characterization of its detailed structure. In contrast, **1** was found to be readily soluble in tetrachloroethane, chloroform, tetrahydrofuran, carbon disulfide, and so on. This allowed us to grow single crystals of **1**, which were obtained by diffusing hexane into a tetrachloroethane solution. SCXRD analysis of **1** revealed a characteristic bilayer structure with a central hexagonal cavity (Fig. 3). The monolayer of **1** could be also regarded as an extended coronoid (*29*); thus, **1** represents as the first bilayer coronoid as well. As shown, **1** contains an inner hole with a diameter of 3.9 Å (Fig. 3A).

Further structural investigation indicated that the two monolayers in **1** adopted a staggered arrangement with a twist angle of 28.8° to minimize the steric hindrance of their peripheral mesityl groups during the stacking. The mean interlayer distance in **1** was measured as 3.4 Å (Fig. 3B), which indicates interlayer π-π interactions. Even with such a staggered orientation, both monolayers in the assembly were slightly bent outward by the repulsion between the mesityl groups of one monomer and the carbon skeleton of the other (as shown as the red dashed line in Fig. 3B and fig. S3). The resultant double-concave structure of **1** could hinder further π-π stacking beyond dimerization to form columnar oligomers. In the crystalline state, **1** packs into a herringbone arrangement with an average interlayer distance of 7.3 Å, which ruled out the possibility of π-π interaction (Fig. 3C), likely due to the steric hindrance imposed by the peripheral mesityl groups.

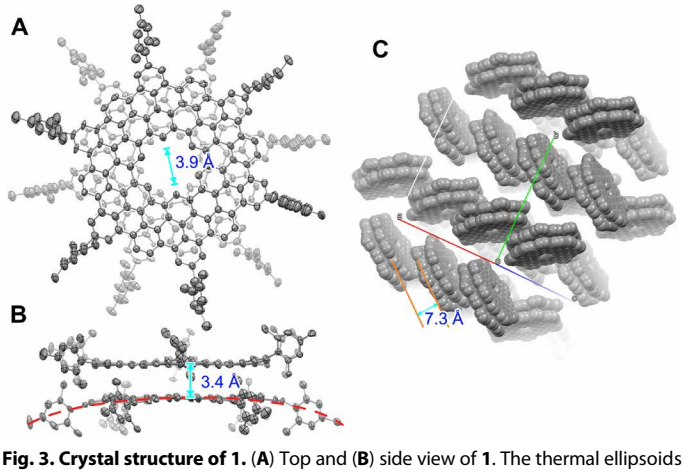

Fig. 3. Crystal structure of 1. (**A**) Top and (**B**) side view of **1**. The thermal ellipsoids are set at a probability level of 50%. (**C**) Packing structure of **1** in a space-filling model without showing the mesityl groups. Hydrogen atoms are omitted for clarity.

Bilayer structure in solution

Many polycyclic aromatic hydrocarbons have been shown to be able to form dimeric structures in the crystalline state, which would dissociate into monomers when dissolved in solution. Therefore, we investigated the structure of **1** in solution by nuclear magnetic resonance (NMR) spectroscopy (Fig. 4). The ^{1}H NMR spectra of **1** consisted of seven singlets with an intensity ratio of 1:4:1:1:3:3:3 (Fig. 4C and fig. S4). The singlet at 12.26 ppm could be assigned to the hydrogens inside the central cavity (designated as H_a). The NMR signal of inner protons (H_a) of **1** is observed at much lower field than that of corresponding protons in kekulene (10.45 ppm) (*29*), which could be attributed to the extended π system of **1**. Note that the two ortho-methyl groups of the mesityl substituent were represented by two ^{1}H NMR signals in the spectrum (H_h, 3.42 ppm, and H_d, 1.87 ppm), suggesting that they were chemically inequivalent (Fig. 4), which was further confirmed by ^{13}C, ^{1}H-^{1}H, and ^{13}C-^{1}H correlation spectroscopy (COSY) NMR spectra (figs. S5 to S7). This, in turn, supported that **1** assumed a bilayer structure in the solution, with one of the above-mentioned ortho-methyl group extending toward and the other away from the interlayer space (Fig. 4). The bilayer architecture of **1** was further corroborated by 2D nuclear Overhauser effect spectroscopy results (fig. S8). Further analysis of **1** by variable-temperature and variable-concentration ^{1}H NMR spectroscopy indicated no obvious alterations, confirming that its bilayer structure was highly stable (figs. S9 and S10). Together, the above results provided convincing evidence that **1** qualified as MDBG in the gas phase, solution, and solid state.

Defect-induced optical modulation

On the basis of its size (2 nm), **1** can be regarded as an atomically precise graphene quantum dot (GQD) (*30*–*33*). GQDs exhibit distinctive optical properties and thus could hold promising potential for applications in imaging, sensing, and optoelectronics (*33*–*37*). However, the factors that govern PL in GQD are still poorly understood (*37*–*39*). For instance, atomically precise GQDs in general emit weak luminescence or even none at all (*30*–*33*), whereas ill-defined

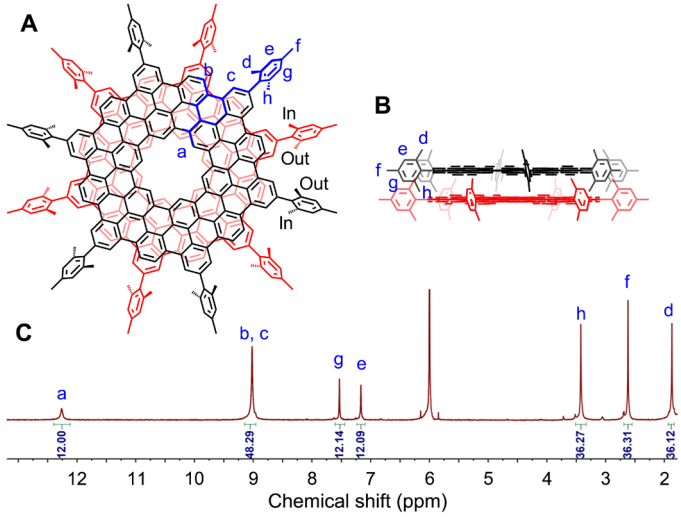

Fig. 4. NMR characterization of 1. (**A**) The top view of **1**. The asymmetric unit is highlighted in blue. "In" and "out" represent the methyl groups in the mesityl substituent that extend toward and away from the interlayer space, respectively. (**B**) The side view of **1**. (**C**) ^{1}H NMR spectrum of **1**. All proton resonances are assigned with the assistance of 2D NMR spectroscopy and theoretically calculated NMR spectrum (figs. S6 to S8).

ones are often much brighter (*34*, *35*). Moreover, most ill-defined GQDs emit at a considerably shorter wavelength than what theoretic calculations based on their sizes would predict (*37*–*39*). To examine the defect-induced optical modulation of GQDs at the atomic level, the optical properties of **1** were compared to those of its same-sized, defect-free counterpart (designated as compound **2**) (Fig. 5 and fig. S11) (*25*). As illustrated, the optical absorption spectra of **1** comprised three peaks at 421, 454, and 496 nm, which could be assigned to the β, p, and α bands, respectively. A comparison between the spectra of **1** and **2** revealed that these absorption bands were blue-shifted by 0.57 to 0.64 eV with the introduction of the inner cavity (Fig. 5B and table S1), causing the color of the solution to change from purple to yellow (Fig. 5C). The optical HOMO-LUMO gap of **1** was calculated to be 2.50 eV, which was much larger than that of **2** (1.93 eV; table S1). These findings provided convincing experimental evidence that hole defects can contribute to bandgap opening in graphenic materials.

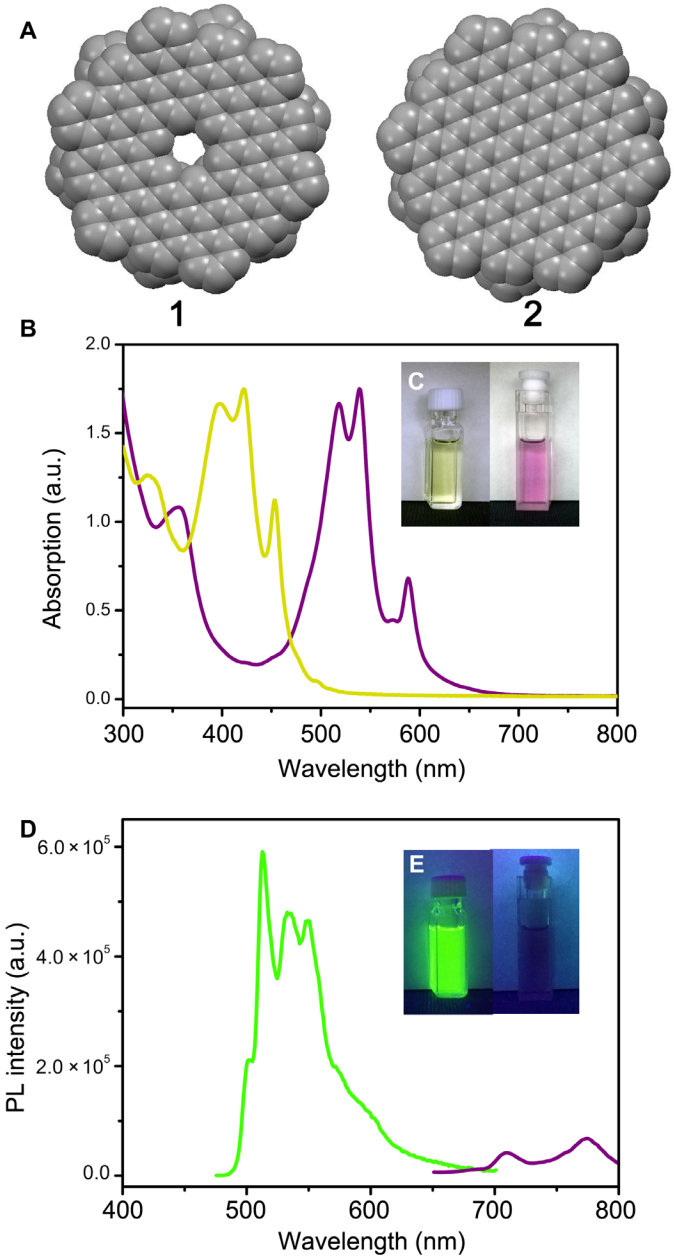

Fig. 5. Optical properties of 1, when compared to the defect-free 2. (**A**) Space-filling model of the inner core of **1** and **2**. (**B**) Absorption spectra of **1** (yellow) and **2** (purple). (**C**) Photographic images of solutions of **1** and **2** under ambient light. (**D**) PL spectra of **1** (green) and **2** (purple). (**E**) Photographic images of solutions of **1** and **2** under ultraviolet light at 365 nm. Photo credits: Yuan-Zhi Tan, Xiamen University.

In addition to the observed alterations in absorption spectra, the highest emission peak of **1** blue-shifted by 255 nm to 512 nm compared to that of **2** (767 nm), although **1** and **2** have the same size (Fig. 5D). Using the emission modulation we observed in **1** and **2** as an atomically precise model, we hypothesized that GQDs synthesized by a top-down approach or by random polymerization could contain lattice defects that enlarge their bandgaps and thus cause their blue-shifted emission, compared to their same-sized, defect-free equivalents. Similar to previously reported atomically precise GQD without defects (*30*–*33*), **2** also shows weak PL (2.6% quantum yield). In contrast, **1** shows a largely brightened emission (Fig. 5E) by 9.6-fold (25.0% quantum yield), which revealed the atomically precise case of defect-enhanced PL for luminescent nanocarbons. To understand the PL enhancement further, the PL dynamics of **1** and **2** were investigated by time-resolved PL spectroscopy. The PL lifetime of **1** and **2** (fig. S12), measured at the maximum emission, was determined to be 54.5 and 28.5 ns (*25*), respectively. On the basis of the PL lifetime and quantum yield, their radiative (k_r) and nonradiative decay (k_{nr}) rate constants were calculated ($k_r = 4.6 \times 10^6\ s^{-1}$ for **1** and $0.91 \times 10^6\ s^{-1}$ for **2**, $k_{nr} = 1.4 \times 10^7\ s^{-1}$ for **1** and $3.4 \times 10^7\ s^{-1}$ for **2**), manifesting a greatly enhanced k_r and a decreased k_{nr} of **1**, which can be responsible for the PL brightening of **1**.

DISCUSSION

A well-defined MDBG was synthesized by rational organic synthesis and rigorously characterized by MALDI-TOF mass spectrometry, NMR spectroscopy, and SCXRD, which confirmed its bilayer structure in gaseous form, solution, and solid state. Compared to its same-sized, defect-free counterpart, the MDBG showed a notable blue shift in both its absorption and PL. A substantial PL brightening of MDBG was observed, which could result from its faster radiative decay and slower nonradiative decay. Together, these results not only demonstrated the utility of defect creation for modulating the optical properties of graphenic materials but also provided an atomically precise model on defect-induced brightening of PL, which will help the understanding and designing of luminescent nanocarbons.

MATERIALS AND METHODS

Synthetic methods

Hexaborylated [6]cyclo-m-phenylene and 2-bromo-5-mesitylbiphenyl were synthesized according to the literature (*25*, *26*).

Synthesis of polyphenylene precursor

A mixture of hexaborylated [6]cyclo-m-phenylene (121 mg), 2-bromo-5-mesitylbiphenyl (840 mg), $Pd_2(dba)_3$ (92 mg), SPhos (82 mg), and Cs_2CO_3 (587 mg) in toluene (6 ml) and water (3 ml) was stirred under argon at 100°C for 24 hours. After cooling, the resulting mixture was washed with water and extracted with CH_2Cl_2 (20 ml, twice).The organic layer was dried by anhydrous $MgSO_4$ and then concentrated

under reduced pressure. The crude products were purified by silica gel column chromatography (dichloromethane/petroleum ether, 1:3), affording the polyphenylene precursor as a white solid (70 mg, 34%).

Synthesis of 1

A solution of polyphenylene precursor (21 mg) in CH_2Cl_2 (21 ml) was degassed by argon bubbling for 10 min. Then, iron(III) chloride (146 mg) was added. After stirring at room temperature for 1 hour with continuous argon bubbling, the reaction was quenched by methanol, and the yellow precipitate formed. The precipitate was collected and purified by silica gel column chromatography (dichloromethane/petroleum ether, 1:1), affording **1** as a yellow solid (6.0 mg, 29%).

Single crystal x-ray diffraction

The crystal was measured on a Rigaku Oxford SuperNova diffractometer, and the temperature of the crystal was controlled by Oxford Cryostream 700. Using Olex2, the initial structure was solved with the SHELX-XT structure solution program using direct method and refined with the XL refinement package using least squares minimization.

Crystal data

Orthorhombic, Pbca (no. 61), a = 33.4310(5) Å, b = 38.4901(11) Å, c = 53.9147(13) Å, V = 69375(3) Å^3, Z = 8, T = 100.00(10) K, $\mu(CuK_\alpha)$ = 1.038 mm^{-1}, 190,854 reflections measured (10.19° ≤ 2Θ ≤ 125.00°), 53,413 unique (R_{int} = 0.1122, R_{sigma} = 0.1162), which were used in all calculations. The final R_1 was 0.1480 [I > 2σ(I)], and wR_2 was 0.3880 (all data).

SUPPLEMENTARY MATERIALS

Supplementary material for this article is available at http://advances.sciencemag.org/cgi/content/full/6/9/eaay8541/DC1

Fig. S1. ^{1}H NMR spectrum of polyphenylene precursor.
Fig. S2. ^{13}C NMR spectrum of polyphenylene precursor.
Fig. S3. Bent structure of **1**.
Fig. S4. ^{1}H NMR spectrum of **1** in $C_2D_2Cl_4$.
Fig. S5. ^{13}C NMR spectrum of **1** in $C_2D_2Cl_4/CS_2$.
Fig. S6. ^{1}H-^{1}H COSY spectrum of **1** in $C_2D_2Cl_4$.
Fig. S7. ^{13}C-^{1}H COSY spectrum of **1** in $C_2D_2Cl_4$.
Fig. S8. H···H proximity in **1**.
Fig. S9. ^{1}H NMR spectra of **1** in $C_2D_2Cl_4$ at different concentrations.
Fig. S10. ^{1}H NMR spectra of **1** in $C_2D_2Cl_4$ at different temperatures.
Fig. S11. Structure of **1** (left) and **2** (right).
Fig. S12. Time-resolved fluorescence spectrum of **1**.
Table S1. Ultraviolet-visible absorption parameters of **1** and **2**.

REFERENCES AND NOTES

1. Y. Zhang, T.-T. Tang, C. Girit, Z. Hao, M. C. Martin, A. Zettl, M. F. Crommie, Y. R. Shen, F. Wang, Direct observation of a widely tunable bandgap in bilayer graphene. *Nature* **459**, 820–823 (2009).
2. L. Ju, L. Wang, T. Cao, T. Taniguchi, K. Watanabe, S. G. Louie, F. Rana, J. Park, J. Hone, F. Wang, P. L. McEuen, Tunable excitons in bilayer graphene. *Science* **358**, 907–910 (2017).
3. H. Patel, R. W. Havener, L. Brown, Y. Liang, L. Yang, J. Park, M. W. Graham, Tunable optical excitations in twisted bilayer graphene form strongly bound excitons. *Nano Lett.* **15**, 5932–5937 (2015).
4. Y. Cao, V. Fatemi, S. Fang, K. Watanabe, T. Taniguchi, E. Kaxiras, P. Jarillo-Herrero, Unconventional superconductivity in magic-angle graphene superlattices. *Nature* **556**, 43–50 (2018).
5. J. González, T. Stauber, Kohn-Luttinger superconductivity in twisted bilayer graphene. *Phys. Rev. Lett.* **122**, 026801 (2019).
6. F. Guinea, N. R. Walet, Electrostatic effects, band distortions, and superconductivity in twisted graphene bilayers. *Proc. Natl. Acad. Sci. U.S.A.* **115**, 13174–13179 (2018).
7. M. Yankowitz, S. Chen, H. Polshyn, Y. Zhang, K. Watanabe, T. Taniguchi, D. Graf, A. F. Young, C. R. Dean, Tuning superconductivity in twisted bilayer graphene. *Science* **363**, 1059–1064 (2019).
8. G. Calogero, N. R. Papior, B. Kretz, A. Garcia-Lekue, T. Frederiksen, M. Brandbyge, Electron transport in nanoporous graphene: Probing the Talbot effect. *Nano Lett.* **19**, 576–581 (2018).
9. A. Fang, K. Kroenlein, D. Riccardi, A. Smolyanitsky, Highly mechanosensitive ion channels from graphene-embedded crown ethers. *Nat. Mater.* **18**, 76–81 (2019).
10. Y. Piao, B. Meany, L. R. Powell, N. Valley, H. Kwon, G. C. Schatz, Y. Wang, Brightening of carbon nanotube photoluminescence through the incorporation of *sp*3 defects. *Nat. Chem.* **5**, 840–845 (2013).
11. J. S. Alden, A. W. Tsen, P. Y. Huang, R. Hovden, L. Brown, J. Park, D. A. Muller, P. L. McEuen, Strain solitons and topological defects in bilayer graphene. *Proc. Natl. Acad. Sci. U.S.A.* **110**, 11256–11260 (2013).
12. M. I. Katsnelson, Scattering of charge carriers by point defects in bilayer graphene. *Phys. Rev. B.* **76**, 073411 (2007).
13. S. Shallcross, S. Sharma, H. B. Weber, Anomalous Dirac point transport due to extended defects in bilayer graphene. *Nat. Commun.* **8**, 342 (2017).
14. J.-S. You, J.-M. Tang, W.-M. Huang, Collective resonances near zero energy induced by a point defect in bilayer graphene. *Sci. Rep.* **8**, 10938 (2018).
15. J. Zhao, G. He, S. Huang, L. F. Villalobos, M. Dakhchoune, H. Bassas, K. V. Agrawal, Etching gas-sieving nanopores in single-layer graphene with an angstrom precision for high-performance gas mixture separation. *Sci. Adv.* **5**, eaav1851 (2019).
16. C. Moreno, M. Vilas-Varela, B. Kretz, A. Garcia-Lekue, M. V. Costache, M. Paradinas, M. Panighel, G. Ceballos, S. O. Valenzuela, D. Peña, A. Mugarza, Bottom-up synthesis of multifunctional nanoporous graphene. *Science* **360**, 199–203 (2018).
17. H. Yoo, R. Engelke, S. Carr, S. Fang, K. Zhang, P. Cazeaux, S. H. Sung, R. Hoyden, A. W. Tsen, T. Taniguchi, K. Watanabe, G.-C. Yi, M. Kim, M. Luskin, E. B. Tadmor, E. Kaxiras, P. Kim, Atomic and electronic reconstruction at the van der Waals interface in twisted bilayer graphene. *Nat. Mater.* **18**, 448–453 (2019).
18. Z. Sun, K. Ikemoto, T. M. Fukunaga, T. Koretsune, R. Arita, S. Sato, H. Isobe, Finite phenine nanotubes with periodic vacancy defects. *Science* **363**, 151–155 (2019).
19. K. Kawasumi, Q. Zhang, Y. Segawa, L. T. Scott, K. Itami, A grossly warped nanographene and the consequences of multiple odd-membered-ring defects. *Nat. Chem.* **5**, 739–744 (2013).
20. T. Fujikawa, Y. Segawa, K. Itami, Synthesis, structures, and properties of π-extended double helicene: A combination of planar and nonplanar π-systems. *J. Am. Chem. Soc.* **137**, 7763–7768 (2015).
21. U. Beser, M. Kastler, A. Maghsoumi, M. Wagner, C. Castiglioni, M. Tommasini, A. Narita, X. Feng, K. Müllen, A C216-nanographene molecule with defined cavity as extended coronoid. *J. Am. Chem. Soc.* **138**, 4322–4325 (2016).
22. Y. Segawa, H. Ito, K. Itami, Structurally uniform and atomically precise carbon nanostructures. *Nat. Rev. Mater.* **1**, 15002 (2016).
23. M. D. Watson, F. Jäckel, N. Severin, J. P. Rabe, K. Müllen, A hexa-*peri*-hexabenzocoronene cyclophane: An addition to the toolbox for molecular electronics. *J. Am. Chem. Soc.* **126**, 1402–1407 (2004).
24. P. J. Evans, J. Ouyang, L. Favereau, J. Crassous, I. Fernández, J. Perles, N. Martín, Synthesis of a helical bilayer nanographene. *Angew. Chem. Int. Ed.* **57**, 6774–6779 (2018).
25. X.-J. Zhao, H. Hou, X.-T. Fan, Y. Wang, Y.-M. Liu, C. Tang, S.-H. Liu, P.-P. Ding, J. Cheng, D.-H. Lin, C. Wang, Y. Yang, Y.-Z. Tan, Molecular bilayer graphene. *Nat. Commun.* **10**, 3057 (2019).
26. K. Ikemoto, A. Yoshii, T. Izumi, H. Taka, H. Kita, J. Y. Xue, R. Kobayashi, S. Sato, H. Isobe, Modular synthesis of aromatic hydrocarbon macrocycles for simplified, single-layer organic light-emitting devices. *J. Org. Chem.* **81**, 662–666 (2016).
27. H. Ito, Y. Segawa, K. Murakami, K. Itami, Polycyclic arene synthesis by annulative π-extension. *J. Am. Chem. Soc.* **141**, 3–10 (2018).
28. H. Ito, K. Ozaki, K. Itami, Annulative π-extension (APEX): Rapid access to fused arenes, heteroarenes, and nanographenes. *Angew. Chem. Int. Ed. Engl.* **56**, 11144–11164 (2017).
29. J. C. Buttrick, B. T. King, Kekulenes, cycloarenes, and heterocycloarenes: Addressing electronic structure and aromaticity through experiments and calculations. *Chem. Soc. Rev.* **46**, 7–20 (2017).
30. M. L. Mueller, X. Yan, J. A. McGuire, L.-s. Li, Triplet states and electronic relaxation in photoexcited graphene quantum dots. *Nano Lett.* **10**, 2679–2682 (2010).
31. X. Yan, X. Cui, L.-s. Li, Synthesis of large, stable colloidal graphene quantum dots with tunable size. *J. Am. Chem. Soc.* **132**, 5944–5945 (2010).
32. M. L. Mueller, X. Yan, B. Dragnea, L.-s. Li, Slow hot-carrier relaxation in colloidal graphene quantum dots. *Nano Lett.* **11**, 56–60 (2011).
33. X. Yan, B. Li, L.-s. Li, Colloidal graphene quantum dots with well-defined structures. *Acc. Chem. Res.* **46**, 2254–2262 (2012).
34. Z. Wang, F. Yuan, X. Li, Y. Li, H. Zhong, L. Fan, S. Yang, 53% Efficient red emissive carbon quantum dots for high color rendering and stable warm white-light-emitting diodes. *Adv. Mater.* **29**, 1702910 (2017).

35. L. Wang, Y. Wang, T. Xu, H. Liao, C. Yao, Y. Liu, Z. Li, Z. Chen, D. Pan, L. Sun, M. Wu, Gram-scale synthesis of single-crystalline graphene quantum dots with superior optical properties. *Nat. Commun.* **5**, 5357 (2014).
36. S. N. Baker, G. A. Baker, Luminescent carbon nanodots: Emergent nanolights. *Angew. Chem. Int. Ed.* **49**, 6726–6744 (2010).
37. X. T. Zheng, A. Ananthanarayanan, K. Q. Luo, P. Chen, Glowing graphene quantum dots and carbon dots: Properties, syntheses, and biological applications. *Small* **11**, 1620–1636 (2015).
38. S. Zhu, Y. Song, X. Zhao, J. Shao, J. Zhang, B. Yang, The photoluminescence mechanism in carbon dots (graphene quantum dots, carbon nanodots, and polymer dots): Current state and future perspective. *Nano Res.* **8**, 355–381 (2015).
39. Z. Gan, H. Xu, Y. Hao, Mechanism for excitation-dependent photoluminescence from graphene quantum dots and other graphene oxide derivates: Consensus, debates and challenges. *Nanoscale* **8**, 7794–7807 (2016).

Acknowledgments: The authors thank Prof. Xu Hou for beneficial discussion. **Funding:** This work was financially supported by the National Natural Science Foundation of China (21771155 and 21721001), the Ministry of Science and Technology of China (2017YFA0204902 and 2018YFA0209500), and the Fundamental Research Funds for the Central Universities (20720180035). **Author contributions:** Y.-Z.T. conceived and designed the project. X.-J.Z., H.H., P.-P.D., Z.-Y.D., Y.-Y.J., Y.-M.L., S.-H. L., and C.T. conducted synthesis and completed the identification. X.-J.Z. and L.-B.F. performed the NMR characterizations. X.-J.Z., H.H., and Y.-Z.T. co-wrote the paper. All authors discussed the results and commented on the manuscript. **Competing interests:** The authors declare that they have no competing interests. **Data and materials availability:** All data needed to evaluate the conclusions in the paper are present in the paper and/or the Supplementary Materials. Additional data related to this paper may be requested from the authors. The atomic coordinates and structure factors have been deposited in the Cambridge Structural Database, Cambridge Crystallographic Data Centre, www.ccdc.cam.ac.uk (accession code, CCDC 1904585).

Submitted 23 July 2019
Accepted 6 December 2019
Published 28 February 2020
10.1126/sciadv.aay8541

Citation: X.-J. Zhao, H. Hou, P.-P. Ding, Z.-Y. Deng, Y.-Y. Ju, S.-H. Liu, Y.-M. Liu, C. Tang, L.-B. Feng, Y.-Z. Tan, Molecular defect-containing bilayer graphene exhibiting brightened luminescence. *Sci. Adv.* **6**, eaay8541 (2020).